

Multiplexed Processing of Quantum Information Across an Ultra-wide Optical Bandwidth

Alon Eldan, Ofek Gilon, Asher Lagimi, Elai Forman, Avi Pe'er*

*Department of Physics and QUEST Center for Quantum Science and Technology,
Bar-Ilan University, Ramat Gan 5290002, Israel*

(Dated: October 30, 2023)

Abstract

Quantum information processing is the foundation of quantum technology. Protocols of quantum information share secrets between two distant parties for secure communication (quantum key distribution), teleport quantum states, and stand at the heart of quantum computation. While various protocols of quantum communication have already been realized, and even commercialized, their communication speed is generally low, limited by the narrow electronic bandwidth of the measurement apparatus in the MHz-to-GHz range, which is orders-of-magnitude lower than the optical bandwidth of available quantum optical sources (10-100 THz). We present and demonstrate an efficient method to process quantum information with such broadband sources *in parallel* over multiplexed frequency channels using parametric homodyne detection for simultaneous measurement of all the channels. Specifically, we propose two basic protocols: A multiplexed Continuous-Variable Quantum Key Distribution (CV-QKD) and A multiplexed continuous-variable quantum teleportation protocol. We demonstrate the multiplexed CV-QKD protocol in a proof-of-principle experiment, where we successfully carry out QKD over 23 uncorrelated spectral channels and show the ability to detect eavesdropping in any of them. These multiplexed methods (and similar) will enable to carry out quantum processing in parallel over hundreds of channels, potentially increasing the throughput of quantum protocols by orders of magnitude.

* avi.peer@biu.ac.il

I. MAIN

In the decades since the conception of quantum information in the 1980s, many practical applications were developed, ranging from secure communications [1–3] and quantum information transmission protocols [4], through quantum sensing schemes [5–8] to quantum computation [9–12]. All these applications rely on non-classical properties of a quantum state, such as entanglement, squeezing, etc., to encode, process and decode the desired quantum information. Examples include various degrees of freedom of light, either in the discrete photon-basis (e.g. polarization [1, 2], spatial mode [13], frequency [14] and time [15]) or in the continuous quadrature-basis (squeezing [6, 16]), as well as material degrees of freedom, such as the energy levels of trapped ions [11] and neutral atoms [12] or the phase / charge of Josephson junctions [17–19].

Two major properties that are often used for optical quantum processing are the optical quadratures of the electric field. Classically, the standard representation of light at frequency ω is $E(t) = |a| \cos(\omega t + \varphi)$ where $a = |a| e^{i\varphi}$ is the complex field amplitude. This field however can be represented also as $E(t) = x \cos(\omega t) + y \sin(\omega t)$ where $x = a + a^*$ and $y = i(a - a^*)$ are the optical quadratures. In quantum optics, these optical quadratures ($x = a + a^\dagger, y = i(a - a^\dagger)$) are non-commuting observables $[x, y] = 2i$, which maintain the canonical quantum uncertainty $\Delta x \Delta y \geq 1$, similar to the canonical position and momentum of quantum mechanics. One can therefore encode quantum information onto the optical quadratures, store, process and decode it.

The focus of this paper is to harness the bandwidth of ultra-broadband optical sources to drastically enhance the rate of quantum optical processing. Most generally, quantum information processing can be broken into three primary stages - generation of the quantum state, manipulation and measurement, where the speed of each stage can be limited by different factors. The primary bottleneck is the measurement, where the relatively slow response of optical detectors limit quantum communication and computation to processing rates that are several orders-of-magnitudes lower than the bandwidth of available sources. In particular, sources of broadband squeezed light with 10-100THz of bandwidth (up to an optical octave) are readily available [20, 21], as well as methods of broadband manipulation using pulse shaping in the spectral domain [22, 23]. In contrast, the bandwidth of traditional measurement techniques was always limited by the narrowband electronic response

of optical detectors, in the MHz-to-GHz range. Luckily, this electronic bandwidth limit was recently overcome with the conception of optical parametric homodyne [24], which enables to measure an optical quadrature of interest across a wide, practically unlimited optical spectrum, opening the door to much faster quantum processing. We here wish to embark on the journey to the other side of this door...

We present a general approach for parallel processing of quantum information, encoded across the entire optical spectrum of the quadratures of broadband two mode squeezed light. We assembled a set of tools (see figure 1) to simultaneously generate, manipulate and measure quantum information over multiple frequency channels, up to $10^3 - 10^4$ channels in realistic configurations, limited only by the available optical bandwidth. In our work, these tools helped us to develop a multiplexed quantum teleportation protocol, which can teleport multiple quantum states simultaneously, as well as a multiplexed QKD protocol (BB84-like), which we demonstrated experimentally over 23 spectral channels in parallel. We note however that the presented toolkit is useful far beyond those two examples, and can be used to form multiplexed variations of any existing quantum protocol, thereby enhancing the processing throughput by orders of magnitude.

A. Multiplexed QKD Scheme Overview

As a first example for a multiplexed protocol of quantum communication, let us present (and later demonstrate experimentally) a simple scheme of multiplexed QKD. We note outright at the beginning that this scheme is not intended to be a protocol for immediate practical implementation of ultrafast QKD, and its primary purpose is to illustrate the viability of frequency-multiplexed quantum processing. Our scheme forms a continuous-variable analog of the BB84 protocol using an unseeded SU(1,1) interferometer. Specifically, both Alice and Bob have an unseeded OPA that generates broadband SPDC and a broadband phase modulation device that consists of a Fourier-domain spectral shaper (see figure 2 and caption for details). Since an unseeded SU(1,1) interferometer generates a wide spectrum of signal-idler pairs, the different frequencies within this spectrum can be used as separate QKD channels.

When a pump laser passes through two OPAs in series, the SPDC generation in the 2nd OPA can interfere with the SPDC generation in the 1st OPA, depending on the phase of

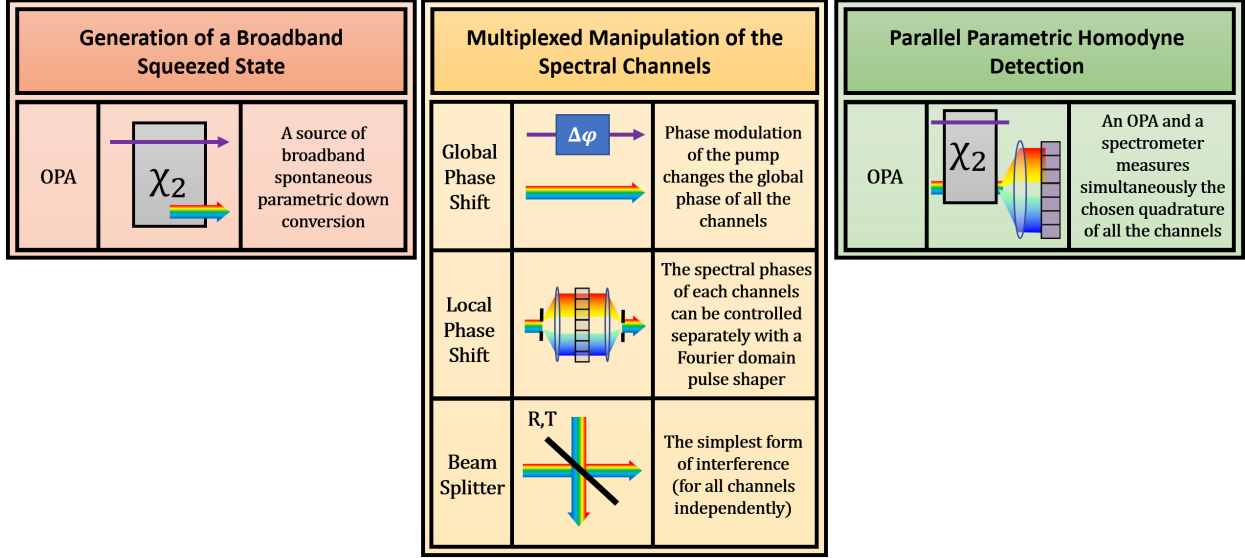


FIG. 1: Our toolset of multiplexed state generation, manipulation and detection used to assemble various quantum protocols (multiplexed QKD and quantum teleportation protocols in this paper): For state generation we use a broadband optical parametric amplifier (OPA), which can generate a broad spectrum of two-mode squeezed light from a narrowband pump. For state manipulation we use phase shifters and beam splitters which help us control the quadratures of the quantum states separately for each channel. Finally, for detection we employ parametric homodyne using another OPA followed by a spectrometer, where the chosen quadrature is amplified and simultaneously measured across the spectrum.

the signal-idler pair relative to the pump. This leads us to the following 4-steps protocol:

1. To encodes her information, Alice modulates the phase of each signal-idler channel in one of two mutually unbiased bases (chosen at random): Basis 1 uses $\phi = 0$ (constructive interference) for logic '1' and $\phi = \pi$ (destructive) for logic '0', whereas basis 2 employs $\phi = \pm \frac{\pi}{2}$. After the spectral modulation of all the channels (in parallel), Alice sends the phase modulated spectrum to Bob.
2. To detect the information, Bob randomly chooses a measurement basis (for each channel separately) using his spectral shaper - by setting the phase to 0 for basis 1 or to $\frac{\pi}{2}$ for basis 2, and passes the light again through his OPA, where the SU(1,1) interference occurs. Bob measures the spectrally resolved light intensity with a spectrometer, which reflects the number of photons in each channel at the output of the complete

SU(1,1) interferometer. If Bob sets the correct basis for a channel, the interference of that channel at the output will be either fully constructive (high probability for photo-detection) or destructive (low probability) and Bob will be able to detect Alice's phase. However, if Bob sets the phase to the wrong basis, his interference will be intermediate, preventing Bob from deducing the information.

3. After the communication is complete, Alice and Bob use a public channel to compare their bases for each channel, keeping only the bits where the encoding and decoding bases matched.
4. Finally, to detect a possible eavesdropper, Alice and Bob compare a fraction of their data, searching for errors that Eve's measurements would have introduced (just like any other QKD protocol).

The security of each channel within this scheme can be analyzed similar to the standard analysis of the BB84 protocol, as summarized hereon (the complete derivation of the security is given in the methods - section II A). Assuming a weak parametric gain in the OPAs, we can employ the perturbative quantum propagator through the nonlinear crystal [25], as $U(t) = e^{iHt} \approx 1 + iHt = 1 + g_\omega a_\omega^\dagger a_{-\omega}^\dagger$, where $a_{\pm\omega}$ represent the field operators of the signal-idler mode pair at $\omega_p/2 \pm \omega$ and g_ω represent the parametric gain of that pair. Assuming the vacuum state as the input to Alice's OPA, the output state after Bob's OPA is

$$|\psi_2\rangle = |0\rangle + g_\omega(1 + e^{i\phi_\omega})|1_\omega, 1_{-\omega}\rangle, \quad (1)$$

where $\phi_\omega = \phi_A + \phi_B$ is the total phase that Alice and Bob apply to the signal-idler pair (relative to the pump field) during steps 1 and 2 of the protocol. The phase $\phi_{A(B)}$ indicates the basis of encoding (measurement) that Alice (Bob) employ for each bit of the channel. The average number of photon that Bob will measure at a specific channel is

$$N_\omega = |\langle 1_\omega | \psi_2 \rangle|^2 = |g_\omega|^2(2 + 2\cos(\phi_\omega)) \quad (2)$$

Notice that when Alice and Bob use different bases, $\phi_\omega = \phi_A + \phi_B = \frac{\pi}{2}/\frac{3\pi}{2}$ and the average number of photons is simply $2|g_\omega|^2$, independent of the phase. However, when the bases match, $\phi_\omega = \phi_A + \phi_B = \pi/0$ the average number of photon equals $0/4|g_\omega|^2$ respectively, so Bob's measurement can decode Alice's information.

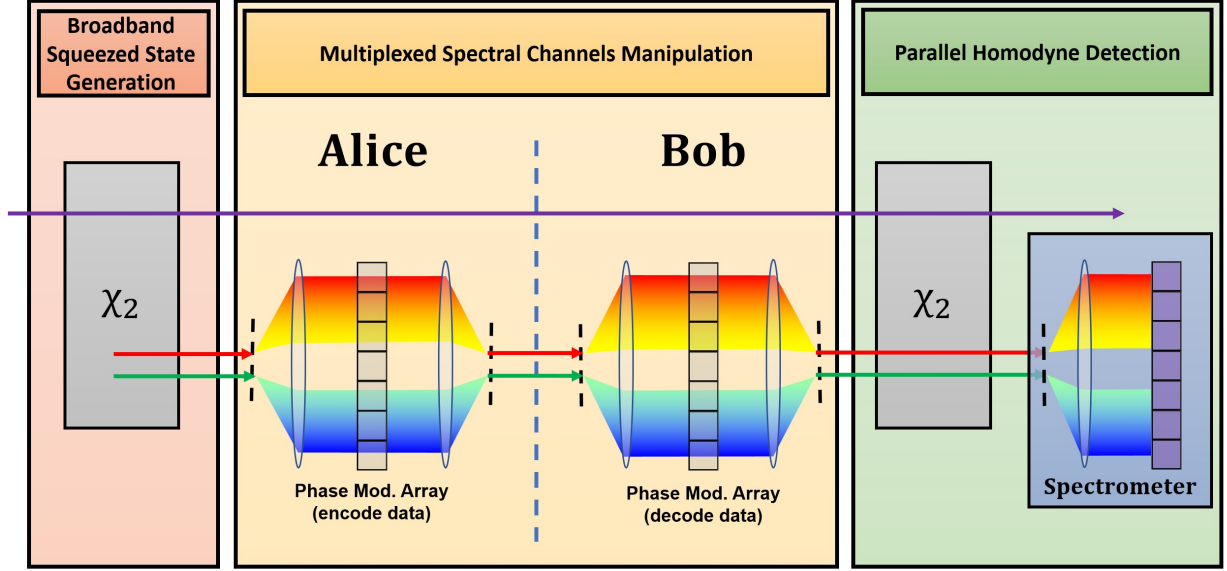


FIG. 2: **The multiplexed QKD protocol.** To encode the data Alice employs a source of broadband, weakly squeezed light (entangled photon pairs) generated using an OPA with broadband phase-matching. Alice modulates the spectral phase of the squeezed light using a Fourier-domain spectral shaper that consists of a spectral separator, such as grating or prism and a spatial light modulator (SLM) to vary the phase of each spectral channel independently. The modulated light is then sent to Bob via an optical fiber. To decode Alice's information, Bob chooses a measurement basis for each channel by modulating the spectral phase of the squeezed light with his spectral shaper (identical to Alice's) and passes the light through a second OPA (completing the $SU(1,1)$ interferometer). Finally, Bob measures the spectral intensity with a spectrometer (the photon-number of each channel).

When Eve tries to attack the communication the situation changes noticeably. For example, if Eve "steals" some of the light using a beam splitter with transmission T , then the number of photons after Bob's OPA becomes (see derivation in the methods, section II A 1)

$$N_\omega = |\langle 1_\omega | \psi_2 \rangle|^2 = |g_\omega|^2 (1 + T + 2T \cos(\phi_\omega)) \quad (3)$$

which diminishes the interference contrast and introduces errors for Bob. Thus, a good discriminator for eavesdroppers is the contrast of the interference after Bob's crystal,

$$V(T) \equiv \frac{I_{max} - I_{min}}{I_{max} + I_{min}} = \frac{2T}{1 + T}. \quad (4)$$

The contrast is a witness for eavesdropping since Eve must steal some of the photons, i.e. reduce the transmission (T) which will lower the contrast. Notice that Eve's ability to extract information relies on a similar interference contrast (in her own measurements), $V_{Eve} = V(R = 1 - T) = \frac{2(1-T)}{2-T}$. Thus, to obtain a sufficient contrast in her measurements, Eve must induce a sufficiently high loss in her beam splitter, which Alice and Bob can later identify.

B. Multiplexed Quantum Teleportation

Multi-channel quantum teleportation, which we propose and analyze here, is another example for harnessing the optical bandwidth to multiplex an important protocol of quantum information. Again we note that this protocol should not be judged as immediately applicable for technology (better implementations will most likely be presented in the future), but rather as an illustration of the range of possibilities that our multiplexing scheme offers for quantum information. This new protocol is a broadband, multiplexed version of the Braunstein's & Kimble's protocol (suggested in [26] and demonstrated in [27]). For this scheme we utilize two sources of broadband squeezed vacuum (OPAs) to simultaneously teleport a set of quantum states across the spectrum of a general broadband field with arbitrary two-mode quadratures at each frequency (see figure 3).

As opposed to the QKD protocol above, which operates in the regime of low squeezing with single pairs of entangled photons, the teleportation protocol we now discuss operates best at the high-squeezing regime. Thus, for the sake of presentation simplicity only, let us assume initially that the two sources are "infinitely squeezed" to the level that we can completely neglect one of their quadratures. Later we will alleviate this assumption and consider the implications of finite squeezing to the teleportation precision. When the two highly squeezed sources (marked (1) and (2) on the figure) are mixed on a beam splitter (BS) with the correct phase, they generate an entangled quantum state, where the quadratures at the two outputs of the BS (marked (3) and (4)) are quantum-correlated. To teleport the input state, we mix it with one of the entangled arms (on another BS) and measure quadratures of the BS outputs (marked (5) and (6)). Based on this measurement, we introduce a quadrature shift (marked (7)) to the unmeasured entangled arm (marked (4)) to reproduce the original quadratures of the input state at the teleportation output (marked

(8)).

To describe the steps of this protocol, we will use the field operator \hat{a}_ω at each frequency which can be decomposed into quadratures as $\hat{a}_\omega = \hat{x}_\omega + i\hat{y}_\omega^\dagger$ (here we use the definition of the two-mode quadratures, $\hat{x}_\omega \equiv \frac{1}{2}(\hat{a}_\omega + \hat{a}_{-\omega}^\dagger)$ and $\hat{y}_\omega \equiv \frac{1}{2i}(\hat{a}_\omega - \hat{a}_{-\omega}^\dagger)$ [28, 29], which is a convenient generalization of the standard single-mode quadratures to the two-mode squeezed pair of signal-idler modes). With this definition, we can represent the input field operator as $\hat{a}_{\omega,in} = \xi(\omega)\hat{x}_\omega + i\eta(\omega)\hat{y}_\omega$ and the field operator of the squeezed state generated by an OPA as $\hat{a}_{\omega,OPA} = X(\omega)\hat{x}_\omega + iy(\omega)\hat{y}_\omega$, where without loss of generality, X represent the stretched two-mode quadrature (at each frequency ω), whereas y represent the squeezing of the other quadrature (dictated by the parametric gain $g(\omega)$ of the squeezers at each frequency, which ideally set $X = e^g, y = e^{-g}$). For convenience, we will drop the frequency index from now on (assuming we look at a specific frequency component of the broad spectrum). Let us now describe in detail each step of this protocol:

1. Two broadband squeezed sources generate two orthogonal squeezed states, $\hat{a}_1 = \sqrt{2}(X\hat{x} + iy\hat{y}^\dagger)$ and $\hat{a}_2 = \sqrt{2}(x\hat{x} + iY\hat{y}^\dagger)$, where X, Y (y, x) are the stretched (squeezed) quadratures of the sources. We will assume that the squeezing is sufficiently high to ensure that the squeezed quadratures are small compared to the input field, i.e. $x \ll \xi$ and $y \ll \eta$.
2. Using a beam splitter, the squeezed states are interfered to generate two quadratures-entangled states, $\hat{a}_3 = \frac{1}{\sqrt{2}}(\hat{a}_1 + \hat{a}_2) \approx X\hat{x} - iY\hat{y}$ and $\hat{a}_4 = \frac{1}{\sqrt{2}}(\hat{a}_1 - \hat{a}_2) \approx X\hat{x} + iY\hat{y}$, where x, y are neglected for now.
3. The broadband input state that we wish to teleport, represented by the field operator $\hat{a}_{in} = \xi\hat{x} + i\eta\hat{y}$, is mixed with one of the entangled beams \hat{a}_3 using a second beam splitter to obtain the encoded states, $\hat{a}_5 \approx \frac{1}{\sqrt{2}}(\xi - X)\hat{x} + \frac{i}{\sqrt{2}}(\eta + Y)\hat{y}$ and $\hat{a}_6 \approx \frac{1}{\sqrt{2}}(\xi + X)\hat{x} + \frac{i}{\sqrt{2}}(\eta - Y)\hat{y}$.
4. The quadratures of the two encoded states are measured with parametric homodyne measurement simultaneously across the two-mode spectrum, such that the quadrature \hat{x} is measured for \hat{a}_5 and \hat{y} for \hat{a}_6 . As a result, we obtain information on *the difference* of the signals quadrature, $\frac{1}{\sqrt{2}}(\xi - X)(\frac{1}{\sqrt{2}}(\eta - Y))$ without any knowledge of the quadratures themselves.

5. The measurement results of the quadratures are transmitted through a classical channel to the desired teleportation location, where a strong coherent state (effectively classical) is generated from the received measurements according to $\hat{a}_7 \approx \alpha (\xi - X) \hat{x} + i\alpha (\eta - Y) \hat{y}$. To recreate the original input state at the teleportation output, we use this coherent state to shift the quadratures of the remaining part of the entangled state, \hat{a}_4 using a beam splitter with high-transmission ($t \approx 1, r \ll 1$). To this end, we set $\alpha = \frac{t}{r}$, which yields $\hat{a}_8 = t\hat{a}_4 + r\hat{a}_7 \approx \xi\hat{x} + i\eta\hat{y} = \hat{a}_{in}$.

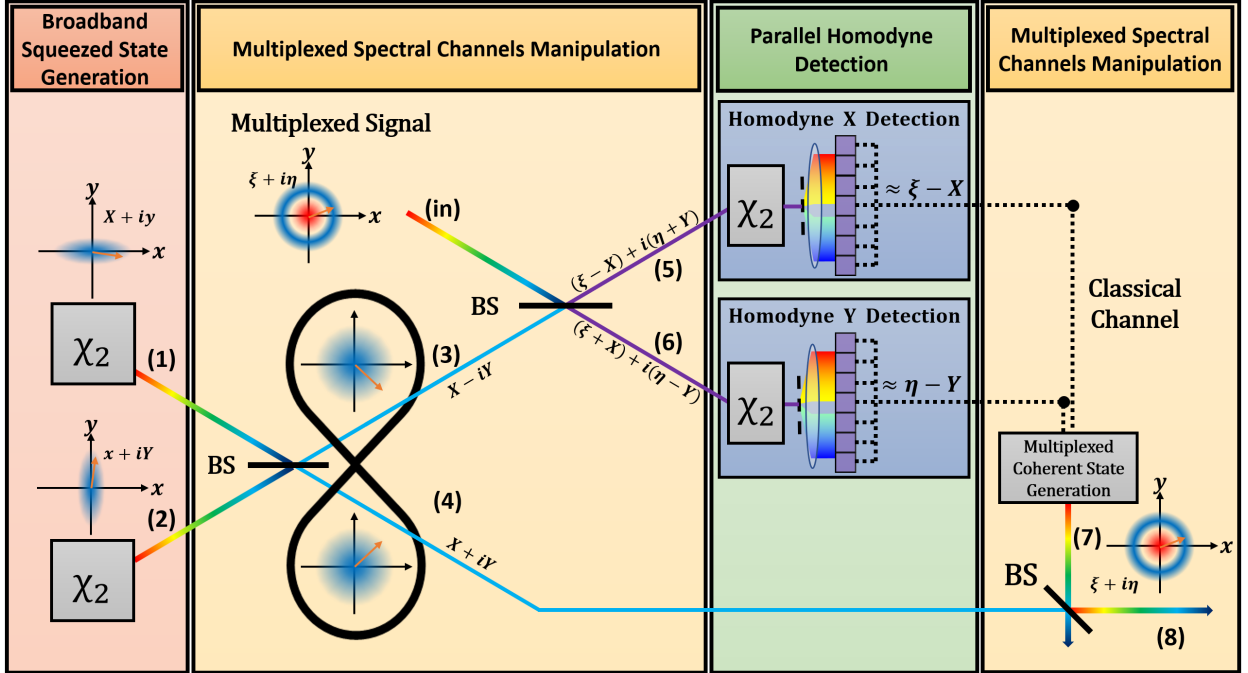


FIG. 3: **The multiplexed quantum teleportation protocol.** Two OPAs are generating two broadband orthogonal squeezed states, squeezed in the \hat{x} and \hat{y} directions (1 and 2). These states are interfered using a beam splitter to produce two quadrature-entangled states (3 and 4). Half of the entangled state (3) is interfered with an input signal (in) using a beam splitter and produces two new complicated states (5 and 6). These states are sent to two orthogonal homodyne detectors, which measure quadratures \hat{x} and \hat{y} respectively to obtain the difference between the entangled state quadratures (4) and the input signal (in). Finally, a coherent state (7) is generated such that it will interfere in a highly unbalanced beam splitter with the rest of the entangled state (4) and shift it to reproduce the original input state at the output (8).

It is important to note that the level of squeezing of the OPAs is a key factor for the fidelity

of the protocol, indicating that the teleportation error is a direct result of the finite squeezing used. If we calculate the output of the protocol \hat{a}_8 without assuming high squeezing, i.e. including also the squeezed quadratures of the OPAs (x, y) , the output operator becomes

$$\hat{a}_8 = t((2x + \xi)\hat{x} + i(2y + \eta)\hat{y}) \approx (2x + \xi)\hat{x} + i(2y + \eta)\hat{y}, \quad (5)$$

indicating that the residue of the squeezed quadratures act as a source of noise, added to the teleportation output. Thus, in order to reduce these errors, it is important to maximize the squeezing of the original signals. For example, one can enhance the squeezing level by replacing the single-pass OPAs in our protocol with multi-pass OPOs (optical parametric oscillator) that offer higher squeezing (up to 15 dB demonstrated [30]).

C. Experimental Results

To demonstrate multiplexed quantum information processing across the optical spectrum we implemented the multi-channel QKD scheme of figure 2 in a proof-of-principle experiment, as outlined in figure 4. Our configuration realized the simultaneous generation, control and measurement of multiplexed QKD frequency channels. The experimental setup is illustrated in figure 4a.

During the experiment the pump passes through the OPA and generates a broadband spectrum of signal and idler pairs across 150nm bandwidth around 1560nm. The pairs are separated from the pump with a Harmonic Separator (H.S) and sent to a spectral shaper to encode Alice's information by modulating the phase of each frequency pair (channel) to $0, \pi$ or $\frac{\pi}{2}, \frac{3\pi}{2}$ randomly (step 1). Simultaneously, the pump passes through an EOM used to stabilize the phase of the pump to that of the pairs, as well as to choose the measurement basis for Bob (same basis for all channels in this case). Finally, the pump and the pairs are reflected back to recombine and pass through the OPA once more in the opposite direction, completing the SU1,1 interference. To implement Bob's parallel detection of all channels we measure the output spectral intensity using a home-built spectrometer composed of a grating and a line CCD-camera (step 2).

To maximize the data capacity while preserving the security of the protocol, the spectral width of the channels at the spectral shaper was chosen to be the smallest possible without leaking to the neighboring channels (see experimental verification in the methods, section

IIB). This allowed us to encode and decode in this preliminary configuration up to 23 channels in parallel with a bare interference contrast of 75%. This 23-fold enhancement of the data capacity (compared to a single channel) is far from any fundamental limit. It can easily be pushed up to > 200 channels by improving the spectral resolution of both the encoding shaper and the spectrometer with standard technology of optical wavelength division multiplexing (see section **IIIA** in the supplementary).

Figure 4b presents the experimental results. To demonstrate our ability to decode the information in both bases, we encoded the 23 channels (at random bases) using the spectral shaper and then, measured them all simultaneously, where in order to select the measurement basis we set the pump-phase to 0 or $\frac{\pi}{2}$. As can be seen, for each measurement the correct basis was detected with good visibility across the entire spectrum, allowing to decode the channels, whereas the channels in the incorrect basis showed no visibility at all. This confirms the ability of Alice and Bob to communicate freely, while preventing attacks on the communication by intercept-resend.

As discussed above, our scheme is a CV, multiplexed version of the well-known BB84 protocol, indicating that all the security proofs of BB84 are directly applicable to our protocol as well. We chose to demonstrate the immunity of our scheme to the steal-attack, i.e. an attempt of Eve to split off some of the light between Alice and Bob, which is a most common attack on QKD. If Eve uses a beam splitter to "steal" part of the quantum state, she inevitably will reduce the interference contrast for Bob. We therefore simulated Eve's operation by introducing loss at the spectral shaper. Although the initial loss in our simple configuration was relatively high (44%, probably due to imperfect components and alignment), we could still clearly detect even a small additional loss of 5% since it visibly reduces the contrast (compared to the measurement error). For more details about the loss detection see the methods, section **IIIC**.

D. Discussion

High data throughput is an important attribute of any information processing scheme. Although the bandwidth of standard broadband sources of squeezed light and entangled photons can easily exceed 10THz (even up to an octave in frequency [21]), the bandwidth resource of the light is yet to be utilized, mainly due to the lack of efficient measurement

techniques with sufficient bandwidth. Our method harnessed optical parametric homodyne in order to efficiently utilize the optical bandwidth to increase the processing capacity by several orders of magnitude. With this method we proposed and demonstrated a multiplexed, BB84-like protocol of QKD, as well as a new quantum teleportation protocol. In spite of the conceptual difference between the teleportation and the QKD applications, they both shared the same set of tools for broadband state generation, broadband state manipulation and broadband state measurement.

If we examine these quantum tools in a broader view, we can realize that they are applicable in the general context of broadband quantum information processing, well beyond QKD and teleportation. An evident example will be to realize frequency multiplexed versions of other protocols of quantum communication, such entanglement-based QKD [3], quantum coin flipping [1], entanglement based sensing [7], etc.. Furthermore, repeating those operations and combining them in various manners is key to implement a broadband quantum network with ultra-fast communication speed.

Another thrust of possible application is towards high-bandwidth quantum computation. Specifically, the ability to simultaneously generate, control and measure a large set of separated squeezed qubits (implemented as signal-idler pairs, as presented above), along with a multiplexed two-qubit operation, is sufficient for universal quantum computation that will exploit the frequency dimension to generate much larger entangled states with the same squeezing resources [31–33]. Note that a multiplexed two-qubit gate was already demonstrated across the quantum frequency comb of a broadband OPO, that is either pumped by several frequencies [31] or phase-modulated in time [34]. Such a multiplexed quantum computer will be naturally compatible with the multiplexed quantum network, mentioned above.

-
- [1] Charles H. Bennett and Gilles Brassard. Quantum cryptography: Public key distribution and coin tossing. *Theoretical Computer Science*, 560:7–11, 2014. Theoretical Aspects of Quantum Cryptography – celebrating 30 years of BB84.
- [2] Sarika Mishra, Ayan Biswas, Satyajeet Patil, Pooja Chandravanshi, Vardaan Mongia, Tanya Sharma, Anju Rani, Shashi Prabhakar, S Ramachandran, and Ravindra P Singh. Bbm92 quantum key distribution over a free space dusty channel of 200 meters. *Journal of Optics*, 24(7):074002, may 2022.
- [3] Artur K. Ekert. Quantum cryptography based on bell’s theorem. *Phys. Rev. Lett.*, 67:661–663, Aug 1991.
- [4] Charles H. Bennett, Gilles Brassard, Claude Crépeau, Richard Jozsa, Asher Peres, and William K. Wootters. Teleporting an unknown quantum state via dual classical and einstein-podolsky-rosen channels. *Phys. Rev. Lett.*, 70:1895–1899, Mar 1993.
- [5] Carlton M. Caves. Quantum-mechanical noise in an interferometer. *Phys. Rev. D*, 23:1693–1708, Apr 1981.
- [6] Wenjiang Fan, Benjamin J. Lawrie, and Raphael C. Pooser. Quantum plasmonic sensing. *Phys. Rev. A*, 92:053812, Nov 2015.
- [7] Yi Xia, Aman R. Agrawal, Christian M. Pluchar, Anthony J. Brady, Zhen Liu, Quntao Zhuang, Dalziel J. Wilson, and Zheshen Zhang. Entanglement-enhanced optomechanical sensing. *Nature Photonics*, 17(6):470–477, Jun 2023.
- [8] Xueshi Guo, Casper R. Breum, Johannes Borregaard, Shuro Izumi, Mikkel V. Larsen, Tobias Gehring, Matthias Christandl, Jonas S. Neergaard-Nielsen, and Ulrik L. Andersen. Distributed quantum sensing in a continuous-variable entangled network. *Nature Physics*, 16(3):281–284, Mar 2020.
- [9] Paul Benioff. The computer as a physical system: A microscopic quantum mechanical hamiltonian model of computers as represented by turing machines. *Journal of Statistical Physics*, 22(5):563–591, May 1980.
- [10] Frank Arute, Kunal Arya, Ryan Babbush, Dave Bacon, Joseph C. Bardin, Rami Barends, Rupak Biswas, Sergio Boixo, Fernando G. S. L. Brandao, David A. Buell, Brian Burkett, Yu Chen, Zijun Chen, Ben Chiaro, Roberto Collins, William Courtney, Andrew Dunsworth,

- Edward Farhi, Brooks Foxen, Austin Fowler, Craig Gidney, Marissa Giustina, Rob Graff, Keith Guerin, Steve Habegger, Matthew P. Harrigan, Michael J. Hartmann, Alan Ho, Markus Hoffmann, Trent Huang, Travis S. Humble, Sergei V. Isakov, Evan Jeffrey, Zhang Jiang, Dvir Kafri, Kostyantyn Kechedzhi, Julian Kelly, Paul V. Klimov, Sergey Knysh, Alexander Korotkov, Fedor Kostritsa, David Landhuis, Mike Lindmark, Erik Lucero, Dmitry Lyakh, Salvatore Mandrà, Jarrod R. McClean, Matthew McEwen, Anthony Megrant, Xiao Mi, Kristel Michielsen, Masoud Mohseni, Josh Mutus, Ofer Naaman, Matthew Neeley, Charles Neill, Murphy Yuezhen Niu, Eric Ostby, Andre Petukhov, John C. Platt, Chris Quintana, Eleanor G. Rieffel, Pedram Roushan, Nicholas C. Rubin, Daniel Sank, Kevin J. Satzinger, Vadim Smelyanskiy, Kevin J. Sung, Matthew D. Trevithick, Amit Vainsencher, Benjamin Villalonga, Theodore White, Z. Jamie Yao, Ping Yeh, Adam Zalcman, Hartmut Neven, and John M. Martinis. Quantum supremacy using a programmable superconducting processor. *Nature*, 574(7779):505–510, Oct 2019.
- [11] J. I. Cirac and P. Zoller. Quantum computations with cold trapped ions. *Phys. Rev. Lett.*, 74:4091–4094, May 1995.
- [12] Harry Levine, Alexander Keesling, Giulia Semeghini, Ahmed Omran, Tout T. Wang, Sepehr Ebadi, Hannes Bernien, Markus Greiner, Vladan Vuletić, Hannes Pichler, and Mikhail D. Lukin. Parallel implementation of high-fidelity multiqubit gates with neutral atoms. *Phys. Rev. Lett.*, 123:170503, Oct 2019.
- [13] Davide Bacco, Yunhong Ding, Kjeld Dalgaard, Karsten Rottwitt, and Leif Katsuo Oxenløwe. Space division multiplexing chip-to-chip quantum key distribution. *Scientific Reports*, 7(1):12459, Sep 2017.
- [14] Matthieu Bloch, Steven W. McLaughlin, Jean-Marc Merolla, and Frédéric Patois. Frequency-coded quantum key distribution. *Opt. Lett.*, 32(3):301–303, Feb 2007.
- [15] Damien Stucki, Nicolas Brunner, Nicolas Gisin, Valerio Scarani, and Hugo Zbinden. Fast and simple one-way quantum key distribution. *Applied Physics Letters*, 87(19):194108, 11 2005.
- [16] Lars S. Madsen, Vladyslav C. Usenko, Mikael Lassen, Radim Filip, and Ulrik L. Andersen. Continuous variable quantum key distribution with modulated entangled states. *Nature Communications*, 3(1):1083, Sep 2012.
- [17] Alexander Shnirman, Gerd Schön, and Ziv Hermon. Quantum manipulations of small josephson junctions. *Phys. Rev. Lett.*, 79:2371–2374, Sep 1997.

- [18] D.V. Averin. Adiabatic quantum computation with cooper pairs. *Solid State Communications*, 105(10):659–664, 1998.
- [19] Lev B. Ioffe, Vadim B. Geshkenbein, Mikhail V. Feigel'man, Alban L. Fauchère, and Gianni Blatter. Environmentally decoupled sds -wave josephson junctions for quantum computing. *Nature*, 398(6729):679–681, Apr 1999.
- [20] C. Manzoni, S.-W. Huang, G. Cirmi, P. Farinello, J. Moses, F. X. Kärtner, and G. Cerullo. Coherent synthesis of ultra-broadband optical parametric amplifiers. *Opt. Lett.*, 37(11):1880–1882, Jun 2012.
- [21] Nir Nechushtan, Hanzhong Zhang, Mallachi Meller, and Avi Pe'er. Optimal detection of ultra-broadband bi-photons with quantum nonlinear $su(1,1)$ interference. *New Journal of Physics*, 23(11):113003, oct 2021.
- [22] Bhaskar Kanseri, Gyaprasad, and Ateesh Kumar Rathi. Broadband spectral shaping using nematic liquid crystal. *Results in Physics*, 12:531–534, 2019.
- [23] Stefano Bonora, Daniele Brida, Paolo Villoresi, and Giulio Cerullo. Ultrabroadband pulse shaping with a push-pull deformable mirror. *Opt. Express*, 18(22):23147–23152, Oct 2010.
- [24] Yaakov Shaked, Yoad Michael, Rafi Z. Vered, Leon Bello, Michael Rosenbluh, and Avi Pe'er. Lifting the bandwidth limit of optical homodyne measurement with broadband parametric amplification. *Nature Communications*, 9(1):609, Feb 2018.
- [25] Yaakov Shaked, Roey Pomerantz, Rafi Z Vered, and Avi Pe'er. Observing the nonclassical nature of ultra-broadband bi-photons at ultrafast speed. *New Journal of Physics*, 16(5):053012, may 2014.
- [26] Samuel L. Braunstein and H. J. Kimble. Teleportation of continuous quantum variables. *Phys. Rev. Lett.*, 80:869–872, Jan 1998.
- [27] Nobuyuki Takei, Takao Aoki, Satoshi Koike, Ken-ichiro Yoshino, Kentaro Wakui, Hidehiro Yonezawa, Takuji Hiraoka, Jun Mizuno, Masahiro Takeoka, Masashi Ban, and Akira Furusawa. Experimental demonstration of quantum teleportation of a squeezed state. *Phys. Rev. A*, 72:042304, Oct 2005.
- [28] Leon Bello, Yoad Michael, Michael Rosenbluh, Eliahu Cohen, and Avi Pe'er. Broadband complex two-mode quadratures for quantum optics. *Opt. Express*, 29(25):41282–41302, Dec 2021.
- [29] Yun Zhang, Hai Wang, Xiaoying Li, Jietai Jing, Changde Xie, and Kunchi Peng. Experimental

- generation of bright two-mode quadrature squeezed light from a narrow-band nondegenerate optical parametric amplifier. *Phys. Rev. A*, 62:023813, Jul 2000.
- [30] Henning Vahlbruch, Moritz Mehmet, Karsten Danzmann, and Roman Schnabel. Detection of 15 db squeezed states of light and their application for the absolute calibration of photoelectric quantum efficiency. *Phys. Rev. Lett.*, 117:110801, Sep 2016.
 - [31] Moran Chen, Nicolas C. Menicucci, and Olivier Pfister. Experimental realization of multipartite entanglement of 60 modes of a quantum optical frequency comb. *Phys. Rev. Lett.*, 112:120505, Mar 2014.
 - [32] Nicolas C. Menicucci, Steven T. Flammia, and Olivier Pfister. One-way quantum computing in the optical frequency comb. *Phys. Rev. Lett.*, 101:130501, Sep 2008.
 - [33] Olivier Pfister. Continuous-variable quantum computing in the quantum optical frequency comb. *Journal of Physics B: Atomic, Molecular and Optical Physics*, 53(1):012001, nov 2019.
 - [34] Xuan Zhu, Chun-Hung Chang, Carlos González-Arciniegas, Avi Pe’er, Jacob Higgins, and Olivier Pfister. Hypercubic cluster states in the phase-modulated quantum optical frequency comb. *Optica*, 8(3):281–290, Mar 2021.
 - [35] 48. 0, 0.

II. METHODS

A. Security Analysis of Frequency-Multiplexed QKD

In section I A of the main text above, we proposed a frequency-multiplexed QKD scheme that employs broadband squeezing and broadband quantum detection, and described its use to share information securely between Alice and Bob using the phases of multiple frequency channels. The security of these channels relies on the ability to efficiently detect eavesdroppers, which requires to identify a difference between the quantum state with and without an eavesdropper (and to measure this difference). For an undisturbed system, the output state is given by equation 1 (section I A),

$$|\psi_2\rangle = |0\rangle + g_\omega(1 + e^{i(\phi_A + \phi_B)}) |1_\omega, 1_{-\omega}\rangle, \quad (6)$$

which yields the detection-probability of photons (phase-dependent) in mode ω , as given by equation 2 (section I A),

$$N_\omega = |g_\omega|^2(2 + 2\cos(\phi_A + \phi_B)). \quad (7)$$

In what follows, we analyze how this output measurement will change under two major attacks - the steal attack and the intercept-resend attack, and how these attacks will be reflected in the statistics of the results.

1. Steal Attack

Under a steal attack, Eve tries to "steal" some of the transmitted light by a beam splitter in the channel with a reflection R representing the stolen amplitude. Eve can then try to use her stolen part to obtain some information (even partial) on the generated key. In this case, Eve modifies the transmitted state to Bob by mixing it with another vacuum mode $|0\rangle_2$ through the beam-splitter, resulting in:

$$|\psi\rangle_{BS} = |0\rangle_1 |0\rangle_2 + g_\omega e^{i\phi_A} \begin{bmatrix} t^2 |1_\omega, 1_{-\omega}\rangle_1 |0\rangle_2 \\ -r^2 |0\rangle_1 |1_\omega, 1_{-\omega}\rangle_2 \\ +irt |1_\omega, 0_{-\omega}\rangle_1 |0_\omega, 1_{-\omega}\rangle_2 \\ +irt |0_\omega, 1_{-\omega}\rangle_1 |1_\omega, 0_{-\omega}\rangle_2 \end{bmatrix}, \quad (8)$$

where t, r are the transmission and reflection amplitudes of Eve's beam-splitter ($t^2 + r^2 = 1$).

Then, the quantum state after Bob's OPA becomes:

$$|\psi\rangle_{BS} = |0\rangle_1 |0\rangle_2 + g_\omega e^{i(\phi_A + \phi_B)} \begin{bmatrix} (e^{-i(\phi_A + \phi_B)} + t^2) |1_\omega, 1_{-\omega}\rangle_1 |0\rangle_2 \\ -r^2 |0\rangle_1 |1_\omega, 1_{-\omega}\rangle_2 \\ +irt |1_\omega, 0_{-\omega}\rangle_1 |0_\omega, 1_{-\omega}\rangle_2 \\ +irt |0_\omega, 1_{-\omega}\rangle_1 |1_\omega, 0_{-\omega}\rangle_2 \end{bmatrix}, \quad (9)$$

where the modulation phase, ϕ_B sets Bob's measurement basis. The average number of photons that Bob will measure in mode ω is:

$$N_\omega = |\langle 1_\omega | \psi \rangle|^2 = |g_\omega|^2 (1 + T + 2T \cos(\phi_\omega)) \quad (10)$$

where $T = t^2, R = r^2$ are the transmission / reflection probabilities.

The primary method to detect Eve is through the errors she will induce in the measurements, which appear in two major forms: First, Eve's beam-splitter may steal one photon of an entangled pair, but not the other, which leads to the observation of single photons without a matching twin (i.e. the states $|1_\omega, 0_{-\omega}\rangle$ and $|0_\omega, 1_{-\omega}\rangle$). Since these possibilities cannot exist in the ideal case, they are good indicators for the amount of loss in the communication channel, which we attribute to Eve. The second type of errors is the "information" errors, where the outcome of legitimate measurements is altered. Specifically, photons can be detected even when the interference is destructive, which reduces the interference contrast. Thus, evaluating the contrast of a large set of measurements is a good discriminator, which is given by

$$V \equiv \frac{I_{max} - I_{min}}{I_{max} + I_{min}} = \frac{2T}{1 + T}. \quad (11)$$

The contrast is a witness for eavesdropping since Eve must steal some of the photons, i.e. reduce the transmission (T) which will lower the contrast. Additionally, we can notice that a background signal (such as noises and signals generated by the attacker) will reduce the contrast even further, and so reduce the signal's credibility. Notice that Bob and Alice can easily calculate both I_{max} and I_{min} during the comparison step of our QKD protocol (section [IA](#), step 4). Specifically, when Alice reveals the transmitted states of the compared data, this allows Bob to calculate the average number of photons that he received for constructive (destructive) interference and obtain I_{max} (I_{min}). Note that for Eve to obtain useful information, she must steal a substantial fraction of the light, since the transmission of her beam splitter (from Alice to Bob) acts as the loss value for Eve. For example, stealing 5%

is equivalent to 95% loss for Eve, which results in only $\sim 10\%$ contrast for Eve and provides little information.

2. Intercept-Resend Attack

Intercept-resend attack was introduced originally with the BB84 protocol [1]. During an intercept-resend attack, Eve tries to imitate Alice by reading the quantum state between Alice and Bob and generating a new quantum state according to her measurement, that she sends to Bob.

Following the calculation in section [IA](#), the average number of photons that Eve will measure after her OPA is

$$N_\omega = |g_\omega|^2(2 + 2\cos(\phi_A + \phi_E)), \quad (12)$$

where ϕ_E is the modulated phase by Eve.

We can gain intuition to the limitations of the intercept-resend attack by considering the simplifying assumption that the number of measured photons during each integration time is exactly 1 (in every shot) for constructive interference (and zero for destructive). In this case, Eve cannot gain any information about Alice's basis, since her measurements will always yield either one photon or none, independent of Alice's encoding. Now, exactly as in BB84, if Eve measured in the correct basis, she will know the state correctly and will be able to impersonate Alice perfectly. However, if Eve measured in the incorrect basis, her reading is random and she cannot recover the encoded phase, thereby introducing an error to the channel with probability 0.5. The total error probability per bit is therefore $P_{Err} = 0.25$, as in BB84, which can be detected easily.

B. Channels Uncorrelation Measurement

In our experiment of multiplexed QKD (described in section [IC](#)), we used a $\sim 100\text{nm}$ bandwidth of SPDC to encode and decode 23 QKD channels simultaneously. Those frequency channels were separated and controlled using a pulse shaper, composed of a grating (to spread the spectrum into different angles), a lens, and an SLM to encode the phase (per channel). A spectrometer was used to measure all the channels simultaneously, composed of

a grating, a lens and a line-CCD camera. In theory, the only mechanism for crosstalk may be the finite frequency resolution of the shaper and the spectrometer (due to the diffraction limit). In practice additional technical imperfections in both the SLM and the camera can lead to crosstalk, such as voltage leakage between neighboring pixels on the SLM. Such problems may cause unwanted correlation between neighboring channels, which lead to security problems. To rule out crosstalk between neighboring channels of the experiment (and so ensure the security of our scheme), we measured the correlation between the channels, as shown in figure 5. In optimal conditions of alignment (diffraction-limited resolution for Alice's shaper and for Bob's measurement spectrometer (CCD pixels), with perfect correspondence between them) no correlation was observed between neighboring channels down to the noise floor of our measurement (figure 5a). However, when misalignment was introduced, correlation between neighboring channels appeared in the form of leakage of the phase modulation from one channel into the measurement of the neighboring channel (see figure 5b). This correlation is an example of information leakage that may help an eavesdropper to reveal data on one channel from the measurement of its neighbor.

In addition to security verification, the uncorrelation measurement serves another purpose - to maximize the number of channels for a given experimental configuration. We used this measurement to find the smallest spectral separation between channels that preserves the uncorrelation property, allowing to maximize the number of channels within the available spectrum. Thus, the uncorrelation measurement is an important step in the calibration of our experiment. This resulted in $130\mu m$ wide channels with $30\mu m$ wide gaps between them.

C. Loss Detection

To verify the security of our multiplexed QKD scheme, we demonstrated the detection of eavesdroppers. Experimentally, we identified the steal attack and quantified its detectability. As we have seen in the security analysis above (section II A 1), a steal attack reduces the average number of photons in mode ω to $N_\omega = |g_\omega|^2 (1 + T + 2T \cos(\phi_\omega))$ (eq. 3) which we can measure. However, as we have seen in II A 1), the better detection parameter is the contrast (visibility) of the interference after the second crystal, which is given by $V \equiv \frac{I_{max} - I_{min}}{I_{max} + I_{min}} = \frac{2T}{1+T}$. (eq. 4). The contrast is a good witness for eavesdropping since Eve must

steal some of the photons, i.e. reduce the transmission (T), which will lower the contrast and therefore introduce errors.

Figure 6 shows the measured dependence of the contrast on the loss (equation 4) along with the theoretical curve, with very good agreement, indicating our ability to detect the loss from the contrast. The loss was introduced by amplitude modulation with the SLM. The only fit parameter of the theoretical curve in figure 6 was the initial loss of the channel which turned out to be around 44%. This high loss was probably caused by a combination of the finite diffraction efficiency of the gratings and the SLM, imperfect AR-coating on the optical components, uneven propagation of the pump, the signal and the idler and other practical factors, which can all be improved in future experiments. And yet, we can clearly detect even a small additional loss of 5% since it reduces the contrast visibly (compared to the measurement error). Thus, Eve will be easily detected even with realistic, rather high initial losses. Note that for Eve to obtain useful information, she must steal a substantial fraction of the light since high loss directly affects the amount of data received during the communication.

III. SUPPLEMENTARY INFORMATION

A. Experimental considerations on the Number of Channels

Although the spectrum of our SPDC source is continuous, the effective number of channels is limited by the spectral resolutions of both the shaper and the spectrometer. These spectral resolutions are governed digitally by the available number of pixels on the SLM (or linear CCD camera) within the spectrum and by the analog spectral resolution of the shaper (spectrometer), as dictated by the grating line-density and by the diffraction limit of the lenses. In this section we explain how all these parameters were tuned to optimize the number of channels in our specific experiment, laying out the "points for future improvement" that can serve future experiments.

Let us first consider the spatial width of each channel on the SLM (or spectrometer). In order to make the most out of the available pixels we optimize the diffraction limit of the lens $d \approx 2.44 \frac{\lambda f}{D}$ to match approximately the pixel size. This sets an appropriate focal length for the lenses:

$$f_{lens} \approx 0.4 \frac{d_{pixel} D}{\lambda} \quad (13)$$

Where d is the diameter of the beam at the focal point, λ is the channel wavelength (1560nm in our setup), D is the beam's diameter on the lens and f is the lens focal length.

The second factor to consider is the SPDC spectrum, which is limited by the phase matching bandwidth of the PPLN OPA. To utilize the most of the available SPDC, one needs to span the SPDC spectrum across the entire SLM (camera). For this we need to consider the angular dispersion of the grating on the SPDC spectrum of width 2ω . The diffraction angle θ of the grating adheres to

$$d \sin \theta = \lambda. \quad (14)$$

To first order approximation $\sin \theta \approx \theta$ we obtain

$$d \cdot \theta_{\omega} = \frac{2\pi c}{\omega}, \quad (15)$$

which allows to calculate the angular span of the spectrum as

$$d \cdot \Delta\theta = \frac{2\pi c}{\frac{\omega_p}{2} - \omega} - \frac{2\pi c}{\frac{\omega_p}{2} + \omega} = \frac{4\omega\pi c}{\frac{\omega_p^2}{4} - \omega^2}. \quad (16)$$

Finally, we choose the grating period d , such that the spectrum will cover the spatial span L of the SLM (camera) at the Fourier plane of the lens, which requires that

$$f_{lens} \cdot \Delta\theta = L. \quad (17)$$

Clearly, the aperture of the focusing lenses D must be sufficient to capture the complete angular spectrum of the light ($D > L$). We can now use equation (16) to obtain the optimal grating period:

$$d = \frac{f_{lens}}{L} \frac{4\omega\pi c}{\frac{\omega_p^2}{4} - \omega^2} \quad (18)$$

The final factor to consider is chromatic dispersion. The optical elements in the beam, such as lenses, filters, polarizers, etc. incur chromatic dispersion on the SPDC spectrum due to the variance of the index of refraction with frequency. Specifically, variation of the phase-sum of the signal-idler pair due to dispersion will shift the overall phase of that pair (channel), resulting in a shift of the interference pattern at this channel. Dispersion therefore should be either compensated or calibrated in order to correctly detect the transmitted information. Dispersion correction can be included in two ways: First, for relatively weak dispersion, where the phase variation across the bandwidth of a single channel is negligible, we can use the phase modulation of the SLM to pre-compensate the dispersion of each channel, which for our experiment was sufficient. However, for cases of high dispersion, as may be the case after passage through a long optical fiber, the phase variation across a single channel may no longer be small, which will lead to reduction of the interference contrast, or even to complete wash-out of the spectral interference fringes. In such a case, physical compensation of the dispersion will be necessary (e.g. with a negative-dispersion fiber or with a prism-pair [], etc.).

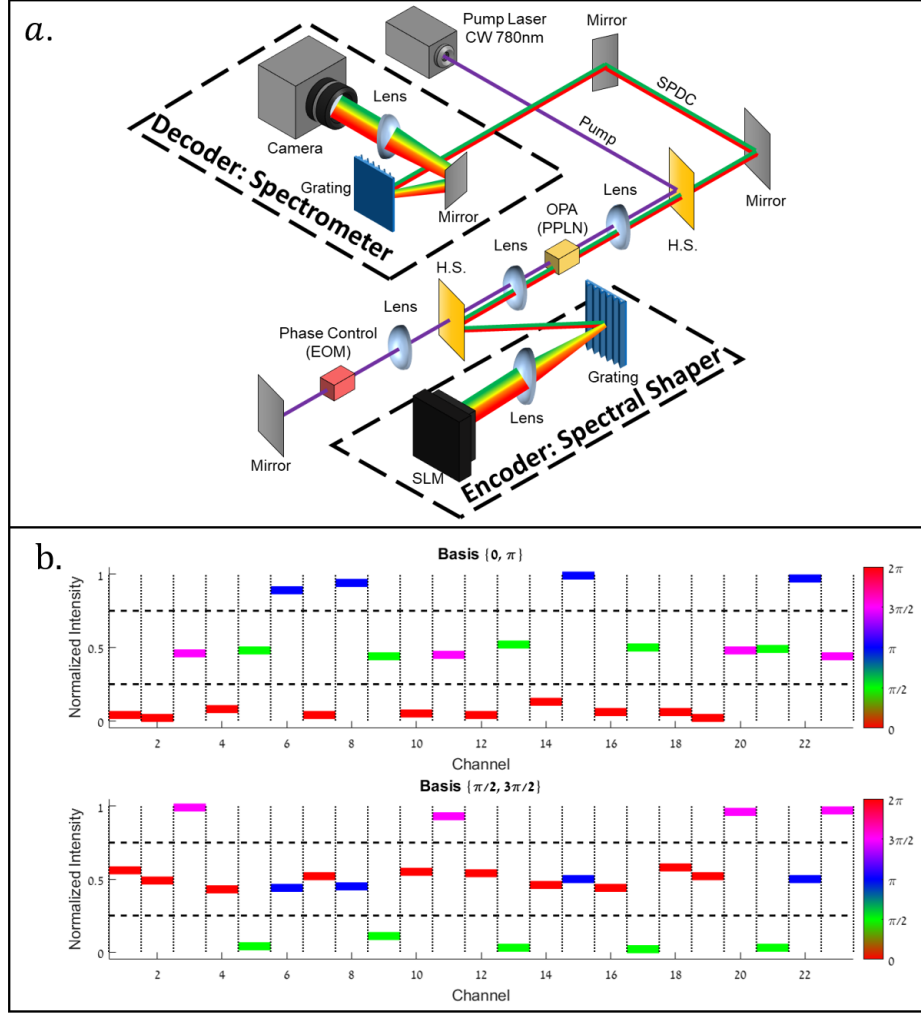


FIG. 4: **Proof-of-principle demonstration of multiplexed QKD:** (a) The experimental configuration. The pump beam (purple) was generated by a CW, single-frequency laser at 780nm of $\sim 1 - 4\text{W}$ output power. The two OPAs of the SU1,1 interferometer were realized in a single periodically polled LiNbO₃ crystal (PPLN in the figure), by passing through the PPLN medium twice: forward for generation of the SPDC photons across a wide spectrum of signal and idler (red and green); and backwards, for parametric homodyne detection. Alice encodes the SPDC light using a spectral shaper for the SPDC and a phase modulator (EOM) for the pump, which is separated off from the SPDC by a harmonic separator (H.S.). To encode information, Alice employs a spectral shaper that consists of a grating, a lens and a spatial light modulator (1x12,288 liquid crystal array SLM). The EOM stabilizes the phase of the pump to that of the SPDC, compensating for phase noise and drifts, by using an active feedback loop (not shown). The EOM also allows Bob to select the measurement basis (same for all channels across the spectrum). Finally, the three beams are reflected back into the OPA crystal, which now acts as Bob's detector. The reflected SPDC light is separated from the pump with another harmonic separator mirror (H.S.) and the resulting SPDC spectrum is recorded on

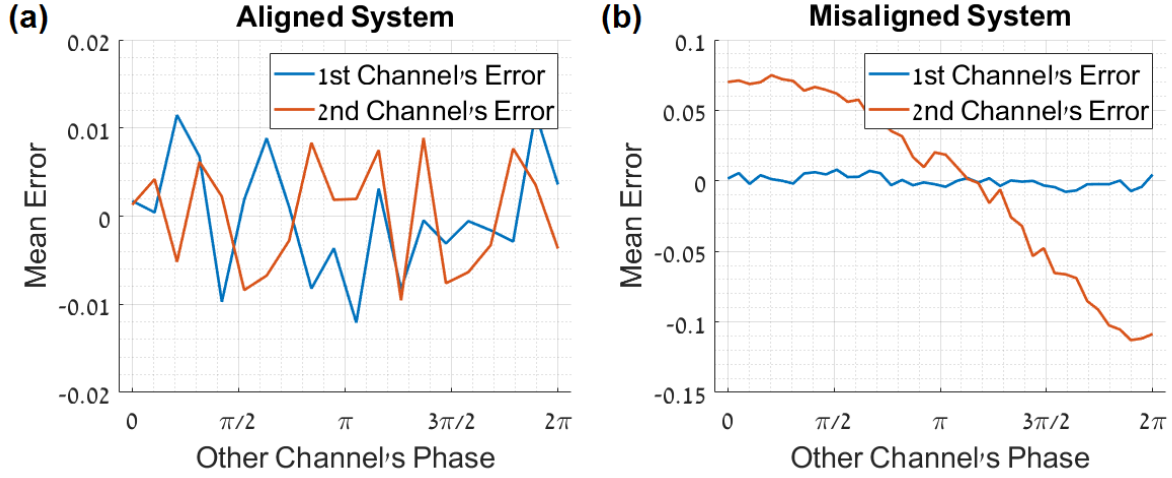


FIG. 5: Cross-talk evaluation: The mean error of one channel $Err_1(\varphi_2) = \langle I_1(\varphi_1, \varphi_2) - \langle I_1(\varphi_1, \varphi_2) \rangle_{\varphi_2} \rangle_{\varphi_1}$ is recorded vs. the phase of its neighbour channel for two cases: **(a)** well aligned channels, where no correlation is observed between the channels down to the measurement noise-floor. **(b)** Misaligned spectral channels, which cause evident dependency between the phase of channel 1 and the measurement of channel 2. **(b)** also shows that correlation errors between neighbour channels are not necessarily symmetrical, depending on the leaks between the channels.

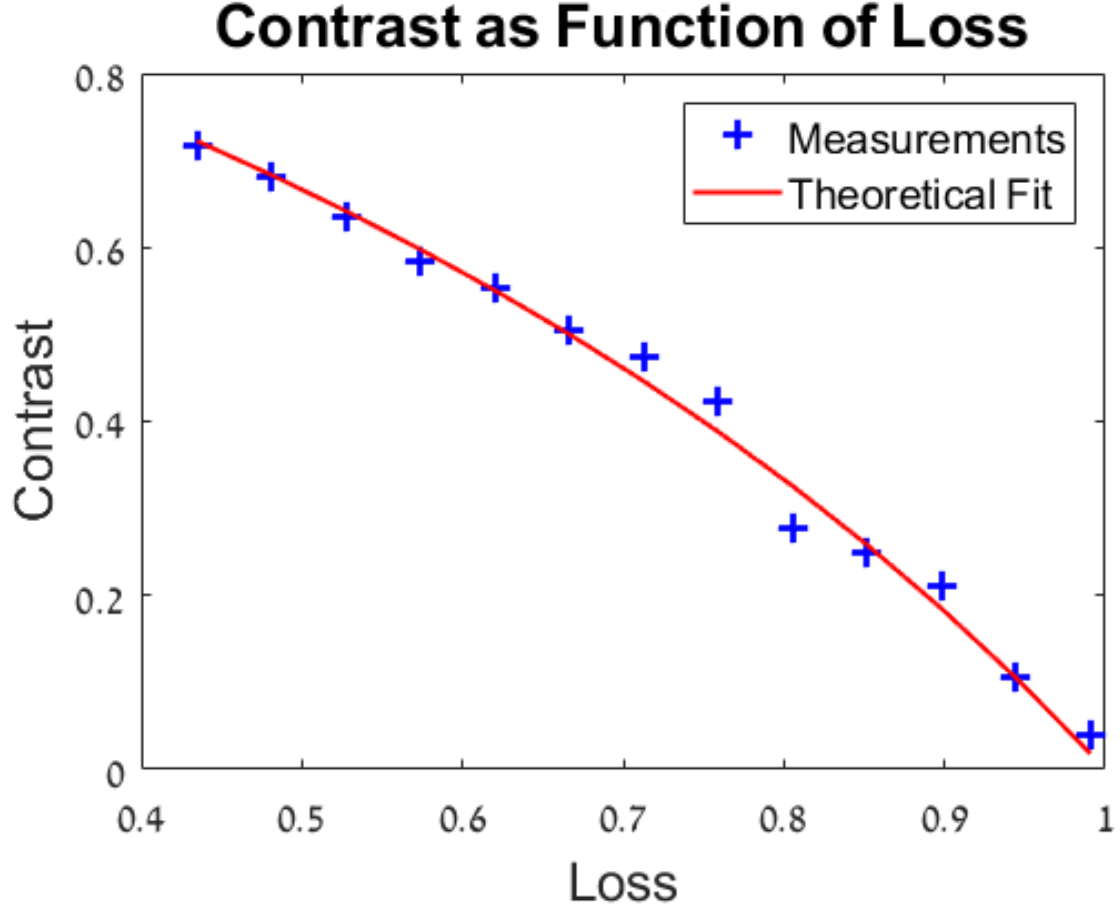


FIG. 6: Detection of steal-attack from measuring the contrast: The figure shows the measured contrast as function of the total transmission loss, which was varied using the SLM (amplitude modulation). Blue crosses show the measured contrast, and the red fit is calculated from equation 4.